Preprint typeset in JINST style - HYPER VERSION

A Novel Self-supporting GEM-based Amplification Structure for a Time Projection Chamber at the ILC

Ties Behnke[a], Ralf Diener[a], Christoph Rosemann[a], Lea Steder[a]*

[a] *DESY,*
Notkestrasse 85, 22607 Hamburg, Germany
E-mail: lea.steder@desy.de

ABSTRACT: In this paper, a new self-supporting way to mount Gas Electron Multipliers is presented. It has been developed to provide a method to cover large readout areas while ensuring the flatness of the foils and keeping the amount of dead material minimal. The structure has been tested in a Time Projection Chamber prototype, using cosmic muon tracks. The impact of the mounting structure on the track reconstruction and the single point resolution is quantified and its impact on the tracking efficiency and dE/dx measurements is estimated.

KEYWORDS: Micropattern gaseous detectors (MSGC, GEM, THGEM, RETHGEM, MHSP, MICROPIC, MICROMEGAS, InGrid, etc); Time projection Chambers (TPC); Detector design and construction technologies and materials; Overall mechanics design.

*Corresponding author

Contents

1. Introduction

A Time Projection Chamber (TPC) is envisaged as the main tracking detector of the International Large Detector (ILD) [1]. The requirements on the design of the ILD TPC are driven by the particle flow concept —described in [1]— and the high precision physics measurements planned at the International Linear Collider (ILC). Most important are an excellent momentum resolution, a very good hit and track efficiency and a very limited amount of material —respectively radiation length— in front of the calorimeters as well as a good hermiticity.

A TPC combines a large number of measurement points with good resolution in three dimensions. This ensures a very robust and efficient pattern recognition. The amplification and readout system for such a TPC needs to provide a large area coverage while introducing a minimum of insensitive regions to allow for a very high particle reconstruction efficiency, i.e. good hit and track reconstruction efficiencies. Further, the required momentum resolution of $9 \times 10^{-5}\,/\mathrm{GeV/c}$ —which translates into a single point resolution of 100 μm [1]— has to be achieved. Finally, homogeneous effective gains have to be ensured to allow for precise dE/dx measurements. Therefore, the flatness of the GEM (Gas Electron Multiplier) foils [2] has to be guaranteed by the mechanical design of the amplification structure.

The support structure described in this paper consists of a light-weight ceramic grid, which ensures a constant distance between the different GEM layers. The grid is glued to the GEM so that the system becomes mechanically stable and scalable to varying numbers of GEMs. With the size

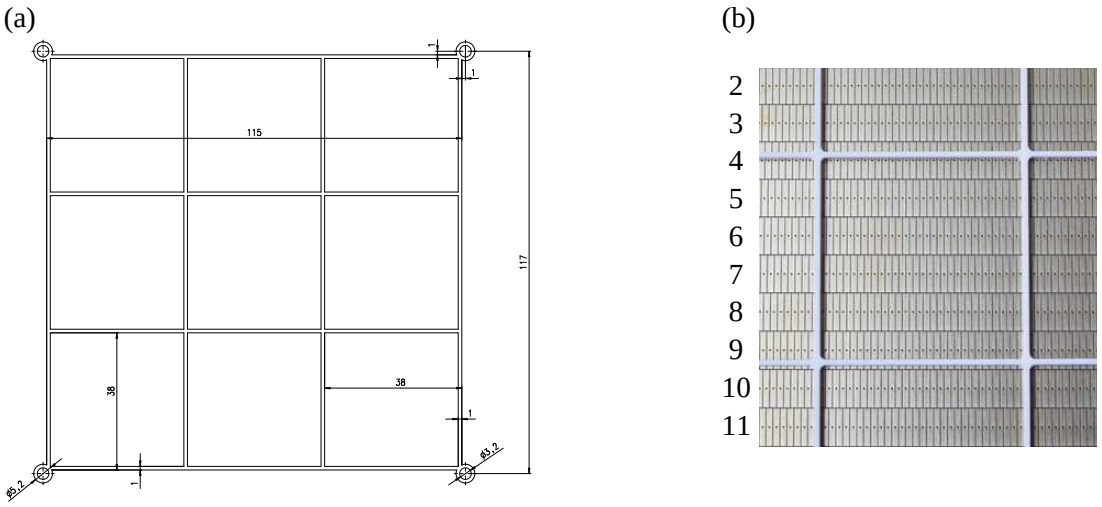

Figure 1. (a) Drawing of ceramics grid, [4]. All measures are given in millimeters. (b) Relative position of grid and pad plane. Row one and twelve are also in the sensitive area of the GEM foils, but not connected due to a limited amount of available readout channels.

of the mesh grid properly chosen, the structure ensures a flat amplification system, which is self-supporting and can be easily mounted on a readout plane with minimal dead zones.
In the following, the design of the support system is described and its impact on the performance of the GEM readout in terms of hit efficiency, tracking performance and single point resolution is studied. Further, its impact on the potential of dE/dx measurements is estimated.

2. Design, Material and Flatness of Grid GEMs

In this section, a new concept to support GEMs with a ceramics grid support is introduced. This structure ensures an equidistant spacing between the GEM foils for transfer and induction gaps.

The support structure is made of an aluminum oxide ceramic (Al_2O_3) [3]. This material is very stiff, an excellent insulator and machinable by laser cutting. A technical drawing of the grids, which were produced to hold standard $10 \times 10\,\mathrm{cm}^2$ GEMs in the medium size TPC prototype at DESY [5], can be seen in figure 1(a). The relevant characteristics are summarized in table 1. The advantage of the grid support is the almost edgeless mounting, which provides the possibility to mount two grid modules very close to each other with only a minimal gap of dead material in between.
The outer dimensions of the grid are chosen to match the environment of the medium size TPC prototype. The restriction to the ratio 1 : 1 for width and height of the bars is given by the current production process. In order to achieve a width of only 1 mm, but a height of 2 mm, which is needed to provide sufficiently large transfer gaps in the GEM stack, two grids were glued on top of each other.
A triple grid GEM stack was produced by gluing GEM foils directly onto the grids with a two-component epoxy resin glue (polybond EP 4619/3 [6]). The grid is only glued on the outer bars to avoid glue stains on the sensitive GEM area. A stretching via heating of the foils is —in contrast to the traditional frame mounting— not necessary. This permits the mounting structure to be thin,

Table 1. Material (96 % Al_2O_3 [3]) and dimensions of grid support structure.

grid support measures	
material	Al_2O_3
radiation length	$X_0 = 7.0\,\mathrm{cm}$
resistivity	$> 10^{12}\,\Omega\mathrm{cm}$
bending strength	$\sigma_B = 350\,\mathrm{MPa}$
outer dimensions	$117 \times 117\,\mathrm{mm}^2$
cell size	$37 \times 37\,\mathrm{mm}^2$
sensitive GEM area	$10 \times 10\,\mathrm{cm}^2$
structure thickness	1 mm
structure height	1 mm

since only small mechanical forces have to be absorbed.
The assembled GEM stack is placed on a readout plane instrumented with pads with a pitch of $1.27 \times 7\,\mathrm{mm}^2$, shown in figure 1(b). Adjacent rows of pads are staggered by half a pad pitch and the grid is aligned to the pads. To study the impact of the grid on the readout performance, the system was placed directly on the pads, without providing un-instrumented areas under the ceramic structure. For the given pad and grid mesh size, in total, about 30 % of the pads are more or less directly affected by the grid. Therefore, it is essential to study the impact the grid has on the performance and to determine the impact on pads close to the grid structure.

The radiation length of aluminum oxide (cf. table 1) has to be compared to $X_0 = 19.4\,\mathrm{cm}$ for glass fiber reinforced plastic (GRP) [7]. However, the bending strength of the ceramic grid allows the surface of the support structure to be built significantly smaller compared to the GRP surface of the traditional mounting frames. This results in a larger solid angle region without dead material inside the detector.

An additional advantage of the new procedure is the flatness of the mounted amplification devices. In [8], a study of conventional mounted GEM surface profiles is presented. The results of this analysis can be summarized in stating, that a flat mounting of GEMs is necessary in order to reach the required dE/dx resolution of smaller than five percent [1].

3. Experimental Setup for Studies of a Grid GEM TPC with Cosmic Muon Data

For the studies, a triple grid GEM stack composed of $10 \times 10\,\mathrm{cm}^2$ GEMs (double conical holes, hole pitch 140 µm) was constructed with the ceramic grids. The stack was operated in a prototype TPC with a drift length of 66 cm at magnetic fields of up to 4 T. The GEM support structure was mounted on top of the readout plane described in section 2. Ten complete pad rows were read out with charge sensitive preamplifiers followed by a 12.5 MHz flash ADC system [9]. As counting gas, the so-called P5 mixture (95 % argon and 5 % methane) was used and the drift field was set to 90 V/cm. The GEMs were used with voltages between 320 V and 325 V. Fields of 1.5 kV/cm were applied in the 2 mm wide transfer gaps, while a field of 3 kV/cm is used in the 3 mm wide induction region. Two scintillator counters operated in coincidence were used to trigger on cosmic muons.
The coordinate system used in the reconstruction is defined by the pad plane —x is pointing hori-

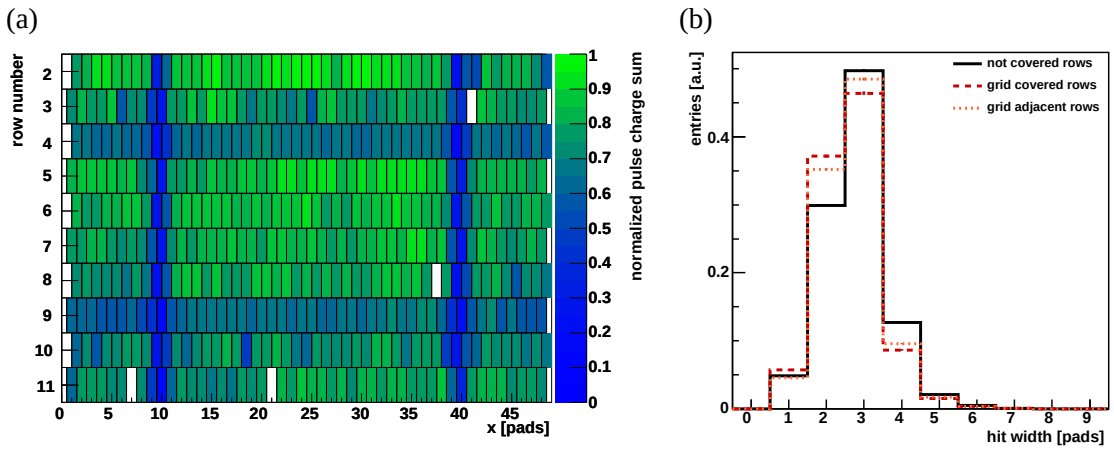

Figure 2. (a) Charge sum —integrated over a complete measurement run— on the readout pads. In each row, pads 9, 10 and pads 39, 40 are covered partly by the vertical grid bars. The horizontal bars are positioned in row four and nine of the pad plane. (b) Influence of the horizontal grid bar on the number of pads contributing to a hit. The distribution has been normalized to the total number of entries. In both figures data measured at a magnetic field of 4 T are shown.

zontally over the pad columns, while y follows the vertical rows— and the drift distance along the chamber axis, corresponding to the z axis.

The data reconstruction is divided in three steps. First, the pad-wise charge deposition from different time bins (corresponding to z values) is combined row-wise by a center of gravity method to three dimensional space points of charge, here denoted by 'hit'. Second, a track finding algorithm is applied, which combines the hits to track candidates. Finally, the tracks are fitted with one of two possible algorithms. More details about the reconstruction algorithms can be found in [10].

4. Grid Impact on Charge Measurement

The charge deposited on a single pad is the starting point for the reconstruction. The impact of the grid on the charge has been studied by investigating the total amount of charge deposited throughout a long data taking period. Assuming that the cosmic rays illuminate the TPC uniformly, any deviations from an uniform distribution can be attributed to the grid structure.

Figure 2(a) shows the charge per pad integrated over a complete measurement run. The structure of the grid is clearly visible through regions of reduced overall charge. The vertical bars, going in the direction of increasing row numbers, cover large fractions of the pad underneath. Due to the staggering, on average close to 50 % of a pad in this region is covered by a grid bar. For the horizontal bars, oriented parallel to the x axis, the bars cover only one out of seven millimeters or about 15 %. The observed reduction in charge per pad is about 25 % for the horizontal bars, and 60 % for the vertical bars, which is in rough agreement with the assumption that the charge reduction is to the first order proportional to the amount of shadowing through the grid. The results show that there exists a clear impact of the grid on the charge deposited on the pads. But by proper choice of the size of the structure and the location of the grid, the impact can be minimized and controlled to

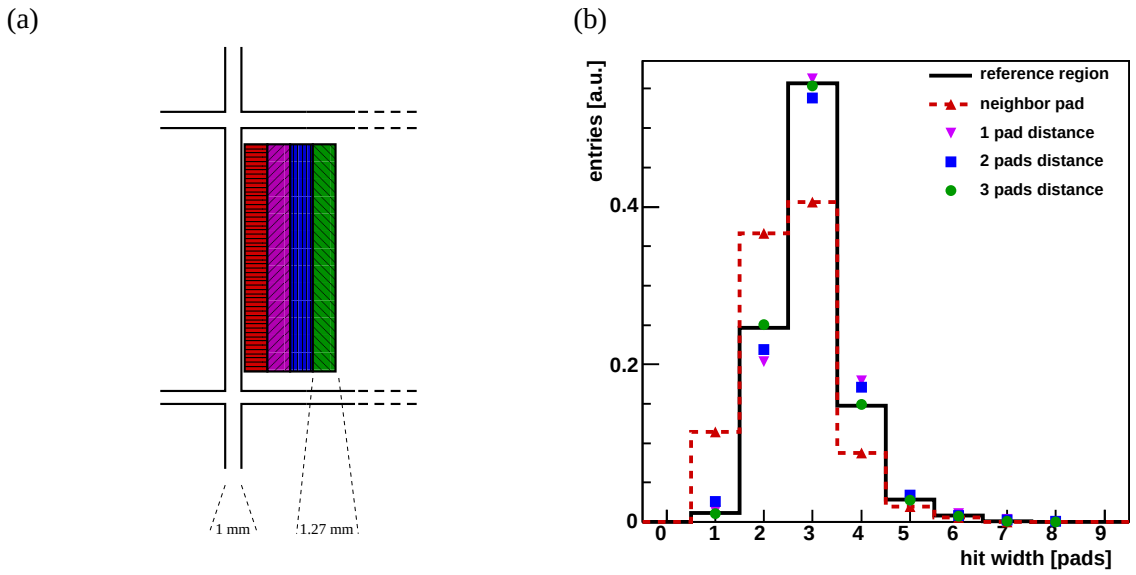

Figure 3. (a) Sketch of the neighboring vertical regions used for comparative studies of the influence of vertical grid bars. Each region has a width of 1.27 mm. (b) Comparison of the number of pads contributing to a hit for the different regions, measured at a magnetic field of 4 T. The distributions are normalized to the number of entries.

a point, that signals from all pads are still present. In the following section, the impact on the hit reconstruction is studied.

5. Grid Impact on Hit Reconstruction and Hit Efficiencies

In this section, aspects of the impact of the grid on hit properties are presented. More details can be found in [8].

Hits are reconstructed within a row, as described in section 3. In figure 2(b) and 3(b) the average number of pads contributing to a hit is shown. The solid histogram shows the distribution for hits which are located in an unaffected area of the pad plane, more than 5 mm away from any grid. Hits reconstructed in an area of the pad plane where a pad is located below a grid are shown in the same plot in the dashed histogram, for an area covered by the horizontal going bar in figure 2(b), for an area covered by the vertical going bar in figure 3(b). In both cases, the average number of pads contributing to a hit is reduced. Close to the grid structure, more two-pad hits occur, which causes a larger uncertainty on the hit position due to using a center of gravity method in the reconstruction [10].

To study how localized this effect is, hits with pads directly adjacent to, or two or three pads away from, a covered pad are studied. For the horizontal going structure, an effect is seen for the covered pad and for the adjacent one, but not beyond. For the vertical going bar as well, only hits on the directly adjacent pads are affected, while hits further away behave essentially as in the reference region.

In the following, the efficiency to reconstruct a hit is defined as the number of reconstructed hits relative to the expected number of hits at this position. To determine the expected number of

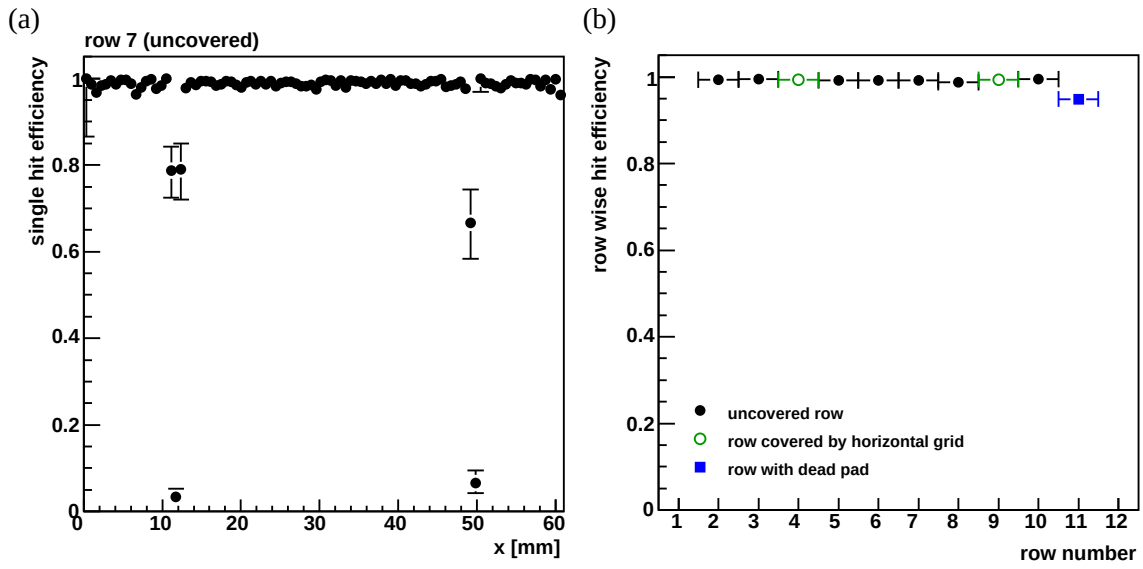

Figure 4. (a) Single hit efficiencies for a row not covered by a horizontal grid bar. The binning corresponds to half a pad pitch. (b) Single hit efficiency as function of the row number. An almost flat distribution can be observed. Only the last row has a slightly lower value due to dead pads in this row. All data measured at a magnetic field of 4 T.

hits, tracks are searched for in the sensitive area. The row for which the hit efficiency is investigated is removed from the track finding and fitting. The expected hit position in the row under investigation is calculated from the parameters of the track. A hit reconstructed in this row is tagged as found if it is within one pad width of the expected hit position.
With the used setup, tracks could have at most 10 rows contributing. To ensure a clean sample of tracks, all rows except the one under investigation are required to show a hit on the track. The hit efficiency as a function of x for row seven (far away from a grid bar) is shown in figure 4(a). A drop in the efficiency is clearly visible for the x regions affected by the vertical grid bars.
In figure 4(b) the same plot is shown as a function of the row number, integrating over all x. The impact of the horizontal going grids in row three and seven is negligible. The last row, number ten, has a lower intrinsic hit efficiency because of two dead pads in this row.

6. Impact of the Grid on the Track Reconstruction

Particle tracks are reconstructed from measured space points by fitting a track hypothesis to these points. In this section, the impact of the grid structures on the point resolution and possible biases in the reconstruction of the points due to the grid are studied. At the end, some considerations are presented about the tracking efficiency and the dE/dx determination.

6.1 Distances

Distances and residuals of hits describe the space between a found hit and the corresponding fitted track. Here, in the case of residuals, the actual hit is excluded from the fit, while for distances the hit is included in the fit. Residuals and distances are used to calculate the single point resolution

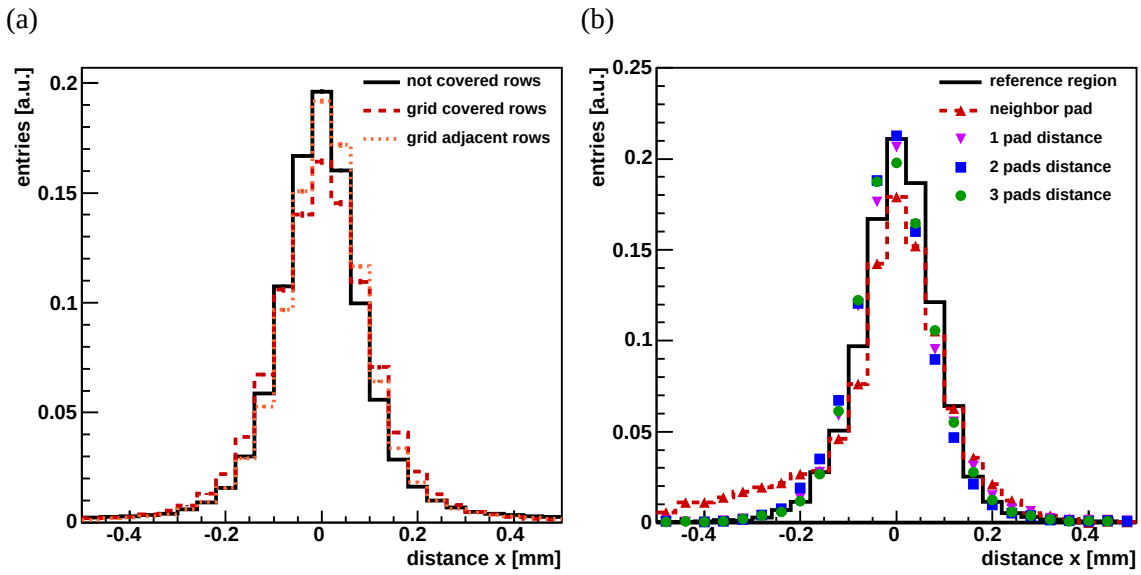

Figure 5. (a) Influence of a horizontal grid bar on the hit distance in x direction. (b) Impact of the vertical grid on the hit distance in x direction. Compared are regions with different distances to a vertical grid bar. All data measured at a magnetic field of 4 T. The distributions are normalized.

with the help of the 'geometric mean method' described in [10]. Here, the impact of the grid on the distances is investigated.

The uncertainty on the hit position for rows covered by a grid structure is larger, since the hit width is smaller. Consequently, these hits get smaller weights in the fitting procedure and are not able to 'pull' the fitted track into their direction as much as hits with smaller uncertainties. In figure 5(a), as before, rows with three types of coverage are compared. As expected, the distances get larger for grid adjacent and grid covered rows.

To assess the impact of the vertical structures, the distribution of distances is shown for the reference sample and the four regions close to the vertical grid bar in figure 5(b). In contrast to the other distributions, the one for the adjacent region is not symmetric with respect to zero, the maximum is slightly shifted towards positive values of x and a tail is present on the negative side. The impact of the grid structure is that hits are 'pushed' away from the bars during the reconstruction. Since only the regions to the right of the grid bars are analyzed, the asymmetry can be explained. The distance distributions of all other regions are symmetric, which confirms that the impact of the grid affects only hits located on directly adjacent pads.

6.2 Single Point Resolution

The single point resolution is an observable of particular importance in tracking detectors. It translates into the momentum resolution of a large scale TPC and gives a handle to judge the performance.

In figure 6(a), the single point resolution is shown for a reference run from a setup using framed GEMs compared with data obtained with grid GEMS. Both measurements were performed in a magnetic field of 4 T and with identical GEM settings. The single point resolution is determined with a χ^2 track fit method including pad response function (PRF) corrections. Details of the method

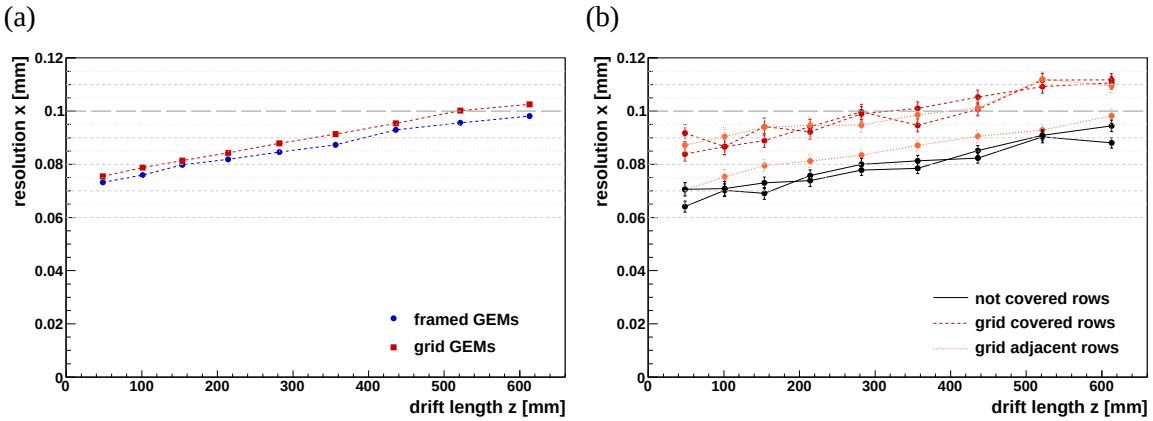

Figure 6. (a) Single point resolution as function of the drift length for a reference data set and a measurement rund with grid GEMs at a magnetic field of 4 T. Both sets (grid/frame) were taken with the same field configuration and ten out of ten possible hits per track were required. (b) Influence of the horizontal grid bars on the single point resolution deduced by the χ^2 method including a pad response correction at a magnetic field of 4 T. Shown are single point resolutions as function of the drift length for six individual rows, two for each case of grid coverage. An impact of the vertical bars is avoided by excluding the outer x regions.

are described in [10]. The tracks are selected according to the cuts summarized in table 2.

Table 2. Track cuts for single point resolution determination.

variable	requirement
number of tracks	$n_{tracks} = 1$
number of hits	$n_{hits} = n_{rows}$
x region	$2.54\,\text{mm} < x_{hit} < 59.06\,\text{mm}$
curvature	$\lvert \kappa \rvert < 0.02\,\text{mm}^{-1}$
inclination in yz-plane	$\lvert \theta \rvert < 0.45\,\text{rad}$
inclination in xy-plane	$\lvert \phi \rvert < 0.1\,\text{rad}$

The differences between both measurements are small —about 5 μm, which is in the range of normal run to run variations.

To draw a conclusion about the impact of the horizontal structures on the single point resolution, the effects of horizontal and vertical bars have to be disentangled. Hence, a harder cut on the x coordinate of hits is made to exclude the outer regions covered by the vertical bars. A safety distance of 3 mm to the vertical bars has been chosen. For a detailed understanding of the impact of horizontal coverage, a comparison of row-wise calculated single point resolutions is presented in figure 6(b). A very clear distinction can be made between rows covered and not covered by the grid, almost 20 μm difference can be observed over the full drift length. The two rows adjacent to the grid show different results. The one closer to the horizontal bar —row ten, cf. figure 1(b)— is much more influenced than row three, whose results are only slightly worse than those of the two reference rows.

A comparison of the single point resolution using all available ten rows, but with the same restric-

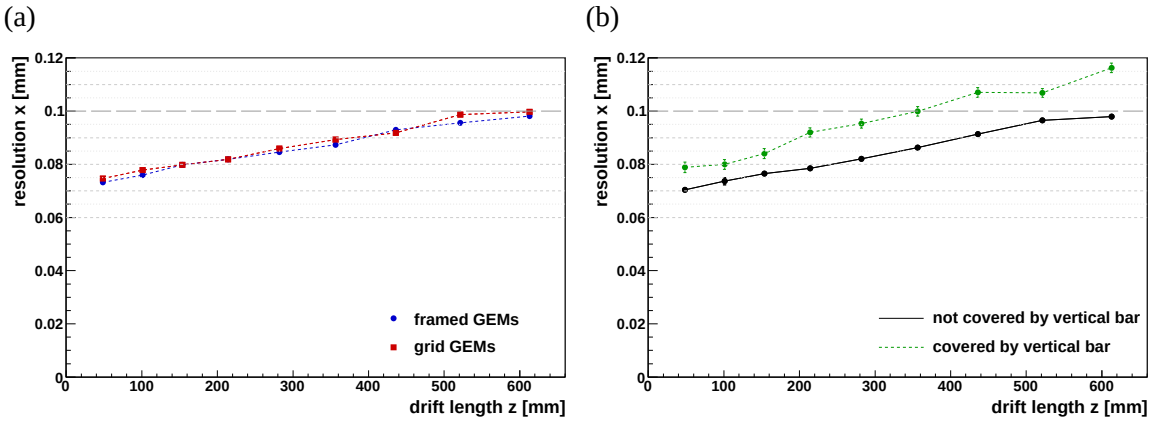

Figure 7. (a) Influence of the horizontal grid bars on the single point resolution as function of the drift length at a magnetic field of 4 T. The region in x is restricted to an area without vertical bars. (b) Single point resolution for regions covered by a vertical grid bar (dashed green) and x ranges, where no vertical bar is shadowing the pad plane (solid black), measured at a magnetic field of 4 T.

tion on the x region, can be seen in figure 7(a). The results show that the horizontal bars have no influence on the measurement as a whole in terms of the single point resolution.

To illustrate the impact of vertical bars on the single point resolution, two sets of different regions of x are compared in figure 7(b). One set includes the x ranges around both vertical grid bars, while the other contains two reference areas of the same width, but uncovered by a vertical bar. Each area has a width of 8.62 mm: 1 mm for the bar itself and three pads to the left and to the right. The width of the areas is defined by the need to be close to the vertical bar in order to be sensitive to the effects and to be wide enough to have large enough statistics to gain reliable results. Furthermore, a certain width is needed to avoid an intrinsic ϕ cut in addition to the ϕ requirement from table 2. For this comparison, tracks with at least six out of ten hits are used. Six hits are needed to ensure stable track fits. Requiring more hits, would exclude tracks influenced by the grid.

A clear difference between the reference and the grid covered regions is visible. The deviations develop from 10 µm at short drift distances to almost 20 µm at the far end of the drift volume. In the case of the covered regions, less statistics is available increasing the uncertainties on the single point resolution.

To summarize the effect on the single point resolution, it can be stated that the overall resolution is not affected in a critical way. The impact of the vertical bars is as expected larger, compared to the one from the horizontal structures, which is negligible. For a large scale TPC, where many hits per track are available, hits close to support structures can safely be excluded from the track fit and by this from the single point and momentum resolution determination.

6.3 Tracking Efficiency and dE/dx Determination

Tracking efficiencies cannot be determined with the prototype assembly used in this paper, since no external reference for the tracks is available. Such studies could be done with the large prototype setup, described in [11, 12], if an external reference system is installed.

Experience from the ALEPH TPC shows, that the tracking efficiency for isolated particles traversing the full radius of the TPC was almost 100 % [13]. For particles in jets with momenta of at least

1 GeV, the tracking efficiency is quoted to be 98.6 %.
The analysis presented here shows that only the vertical bars have an impact on the hit reconstruction in a way, that hits close to the structure are not linked to the corresponding track. All tracks need to have a sufficient number of hits on their way through the chamber, to ensure high tracking efficiencies for the ILD TPC. Hence, in particular straight tracks with a large transverse momentum passing along a sector boundary or support structure bar, require a careful design of staggered readout modules and grid support structures. A track with a transverse momentum of $p_T = 100\,\mathrm{GeV}$ in a magnetic field of 3.5 T has a radius of about 95 m. With such a small curvature, the track stays over a length of 87 cm on a 1 mm wide strip, for example a module border or a grid bar. Since the impact of the grid is limited to at most two pads, an adapted design of the layout of the readout modules with staggered boundaries can ensure a high tracking efficiency even in these regions.
In [8], surface profiles of framed GEMs were measured and a simulation study for the gain uniformity was performed. Tracks recorded in a TPC with such framed GEMs do not show a good enough effective gain homogeneity to reach a dE/dx resolution of 5 % as required in [1]. The improved flatness of GEMs mounted with the grid system (cf. [8]) allows to reach this precision. For dE/dx determination, quality cuts on the hits have to be applied, as described in [14]. These cuts account for various effects and the construction of the chamber. In particular sector boundaries have to be cut out. For the grid support structure, additional geometric cuts have to be introduced.

7. Summary

A novel scheme to support and mount GEM foils inside a TPC has been developed in order to be able to cover a large readout area with the least possible dead material. This self-supporting structure is made of a ceramic grid glued in between the GEM foils. Ceramic is well suited for applications in a TPC due to its electrical and mechanical properties. It is a good insulator and at the same time mechanically very stiff. The material budget can be reduced with respect to mounting GEMs on GRP frames. In addition, a very flat mounting can be achieved without stretching of the GEMs. The new support structure allows a stable operation and has been successfully tested in a medium size TPC prototype.
In order to quantify the impact of the grid GEMs on the track reconstruction, cosmic muons have been recorded in a magnetic field of 4 T. The data analysis has shown that the impact of the ceramic grid will be visible in all steps of the track reconstruction due to a reduction of the measured charge. However, the impact of horizontal and vertical bars —perpendicular and parallel to the longer axis of a readout pad— have to be treated separately. The horizontal structures do not affect the hit efficiency. The single point resolution obtained with grid GEMs covered by horizontal bars is competitive, only for dE/dx determination additional quality cuts will have to be introduced to ensure a reliable measurement. Vertical bars produce shifted hits in their immediate vicinity and the single point resolution is worsened by up to 20 % close to these structures. Hits close to vertical bars have to be removed from dE/dx samples.
However, the benefits outweigh these caveats and can improve the track reconstruction and dE/dx measurements in future GEM TPCs. The advantages of the grid support structure are the minimal amount of material, the achievable flatness without the need of stretching the foils, the almost edgeless module borders and the possibility to cover large areas without significant gaps. The

developed grid mounting structure will allow for the step from small GEM applications —used for proof-of-principle studies— to a large scale GEM TPC in a modern high energy detector like the ILD.

Acknowledgments

This work is supported by the Commission of the European Communities under the 6th Framework Programme 'Structuring the European Research Area', contract number RII3-026126.

References

[1] T. Abe *et al.* [ILD Concept Group - Linear Collider Collaboration], *The International Large Detector: Letter of Intent*, arXiv:1006.3396 [hep-ex].

[2] F. Sauli, *GEM: A new concept for electron amplification in gas detectors*, Nucl. Instrum. Meth. A **386** (1997) 531.

[3] http://www.anceram.com/3_keramik/produktbeschreibung_en.php, *ANCeram Company website - technical ceramics*, 2010

[4] F. Hegner, *private communication*, 2010

[5] T. Lux, *Studies for a time projection chamber for the International Linear Collider and measurement of beauty cross sections in deep inelastic scattering at HERA*, DESY-THESIS-2005-019.

[6] http://www.polytec-pt.com, *Polytec PT company web site – in german*, 2010

[7] W. M. Yao *et al.* [Particle Data Group Collaboration], *Review of Particle Physics*, J. Phys. G **33** (2006) 1.

[8] L. Hallermann, *Analysis of GEM properties and development of a GEM support structure for the ILD Time Projection Chamber*, DESY-THESIS-2010-015.

[9] M. Ball, N. Ghodbane, M. E. Janssen and P. Wienemann, *A DAQ system for linear collider TPC prototypes based on the ALEPH TPC electronics*, LC-DET-2004-013, arXiv:0407.120 [physics]

[10] M. E. Janssen, *Performance studies of a time projection chamber at the ILC and search for lepton flavour violation at HERA II*, DESY-THESIS-2008-011.

[11] T. Behnke, K. Dehmelt, R. Diener, L. Hallermann, T. Matsuda, V. Prahl and P. Schade, *A Lightweight Field Cage for a Large TPC Prototype for the ILC*, JINST **5** (2010) P10011 arXiv:1006.3220 [physics.ins-det].

[12] K. Dehmelt [LCTPC Collaboration], *A large prototype of a time projection chamber for a linear collider detector*, Nucl. Instrum. Meth. A **623** (2010) 97.

[13] W. B. Atwood, T. Barczewski, L. A. T. Bauerdick, L. Bellantoni, E. Blucher, W. Blum, J. Boudreau and O. Boyle *et al.*, *Performance of the ALEPH time projection chamber*, Nucl. Instrum. Meth. A **306** (1991) 446.

[14] M. Hauschild, R. D. Heuer, C. Kleinwort, J. Ludwig, W. Mohr, D. Schaile, O. Schaile and C. Wahl *et al.*, *Particle identification with the OPAL jet chamber*, Nucl. Instrum. Meth. A **314** (1992) 74.